

# Extracting Dynamical Models from Data

Michael F. Zimmer  
zim@neomath.com

October 14, 2021

## Abstract

The FJet approach is introduced for determining the underlying model of a dynamical system. It borrows ideas from the fields of Lie symmetries as applied to differential equations (DEs), and numerical integration (such as Runge-Kutta). The technique can be considered as a way to use machine learning (ML) to derive a numerical integration scheme. The technique naturally overcomes the "extrapolation problem", which is when ML is used to extrapolate a model beyond the time range of the original training data. It does this by doing the modeling in the phase space of the system, rather than over the time domain. When modeled with a type of regression scheme, it's possible to accurately determine the underlying DE, along with parameter dependencies. Ideas from the field of Lie symmetries applied to ordinary DEs are used to determine constants of motion, even for damped and driven systems. These statements are demonstrated on three examples: a damped harmonic oscillator, a damped pendulum, and a damped, driven nonlinear oscillator (Duffing oscillator). In the model for the Duffing oscillator, it's possible to treat the external force in a manner reminiscent of a Green's function approach. Also, in the case of the undamped harmonic oscillator, the FJet approach remains stable approximately  $10^9$  times longer than 4th-order Runge-Kutta.

## 1 Introduction

This paper is concerned with modeling data that arises from a dynamical system. Specifically, the focus here is on using machine learning (ML) for the modeling, with the hope of converting that model into something more insightful, such as a differential equation (DE) and accompanying domain knowledge (such as constants of motion). This endeavor is broken down into these five goals:

1. Extrapolate model beyond training data times.
2. Determine underlying DE.
3. Determine parameter dependencies in DE.
4. Estimate stability/accuracy of model.
5. Determine related domain knowledge.

## Related Work

The previous work of interest here has to do with modeling the nonlinear dynamics of a system, given time series information from measurements. Since the subfield of interest to this paper is also on understanding the underlying dynamics, curve fitting procedures such as time series analysis will not be reviewed as related work.

While previous work really may be traced back to attempts at modeling physical systems, such as by Poincaré [1885], [Holmes, 1990], Poincaré [1993] with his work on celestial mechanics, modern work might be identified as beginning with Packard et al. [1980] in their study of the time series of nonlinear and chaotic time series, and the study by Takens [1981] in turbulence. Not long after this, the work by Crutchfield and McNamara [1987] produced a form of the analysis that would be repeated: the data was fit to a model of the form  $dy/dt = F$ , where the form of  $F$  was guided by minimizing a complexity measure. They considered general dynamical systems, and in particular the examples of the Lorenz model and the Duffing oscillator. A number of other significant works would soon follow, including [Broomhead and Lowe, 1988], [Casdagli, 1989], [Cremers and Hübler, 1987], [Breedon and Hübler, 1990], [Gouesbet, 1992], and others. The techniques that were used in this time period for modeling  $F(y)$  included polynomial expansions, radial basis functions, NNs, B-splines, etc; the reader is referred to the review by Aguirre and Letellier [2009] for a more complete discussion of these works.

In more recent times this problem is receiving renewed attention, this time mainly from the vantage point of recent NN techniques. The common theme has been to enforce a physics prior onto the network, forcing the dynamics to obey it in a *conserved* fashion. For example, [Lutter et al., 2019] introduced a Lagrangian prior on the physics and modeled robot tracking control. This Lagrangian technique was generalised by [Cramer et al., 2020], who considered non-dissipative applications of a double pendulum, relativistic particle, and a 1D wave equation. Also, [Greydanus et al., 2019] used a Hamiltonian prior on the NN and studied conservative systems such as a mass-spring system, a pendulum (ideal and real data). [Toth et al., 2019] introduced Hamiltonian Generative Networks to model conserved densities satisfying Hamiltonian dynamics, which has applications towards image analysis, for example.

Another type of approach [Rudy et al., 2017] is a generalization of the work of Crutchfield on a regularized fit to  $dy/dt = F$ . They used software (SINDy) to analyze the best fit for a dynamical model, and applied it to Navier-Stokes, quantum harmonic oscillator, diffusion equation, and other PDEs. Also, Liu et al. [2021] recently have found how to use NNs to detect the presence of, and model, non-conservative forces in a physics context. Finally, there are other contributions besides these, but space does not permit a more complete discussion.

## Outline

The layout of the paper is that of an Overview (Section 2), three Examples (Section 3, 4, and 5), Final Remarks (Section 6), and three Appendices.

The Overview covers background for the FJet method, which is introduced herein. It covers the scope of dynamical systems being considered here, the basic idea of the

FJet modeling, recommendation for choosing the variables and model, and also how to compute constants of motion making use of ideas from Lie symmetries applied to ODEs. The three Examples are on: damped harmonic oscillator, damped pendulum, and the Duffing oscillator. Their treatments largely follow the same logical progression, as an aid to the reader. After the Final Remarks, there are three Appendices, covering the Runge-Kutta scheme, stability of the harmonic oscillator, and a computation of the integration constant  $r$ , which in this case generalizes the energy for a *damped* harmonic oscillator.

## 2 Overview of FJet Approach

In this section the key issues of the problem and an outline of the solution are discussed.

### 2.1 Scope of Dynamical Systems

In this paper, the emphasis is on seeking to model a deterministic system from noisy observations. Specifically, there is the assumption that there exists an underlying differential equation (DE) that describes it, whether it be an ordinary DE (i.e., ODE) or a partial DE (i.e., PDE). It will generally be assumed that the highest order derivative term in the underlying DE has a unit coefficient. In the context of ODEs this is the Cauchy form; in the context of PDEs this is the Cauchy-Kovalevskaya form [John, 1982, DiBenedetto, 2009]. More precisely, for ODEs the Cauchy form appears as

$$u^{[n]} = A_0(u, t)u + A_1(u, t)u^{[1]} + \dots + A_{n-1}(u, t)u^{[n-1]} \quad (1)$$

where the superscript denotes the derivate wrt the indep variable  $t$ . The functions  $A_i$  ( $i = 0, \dots, n - 1$ ) are taken to be local. However, the nonlocal case, where the DE is an integro-differential equation can in principle also be pursued, but will not be investigated in this paper.

In the models considered herein, time dependence will only enter through a function  $b(t)$ , and the modeling will be done with respect to  $b$ . (In that sense, it is treated like a Green's function). After the model is built, knowledge of  $b(t)$  will be required to make predictions. This is a natural approach for cases such as a driven oscillator, for example.

### 2.2 Mapping Approach

In typical ML approaches for modeling dynamical systems, one is given training data over some finite time interval, and then seeks to model and make predictions over later times. Attempting to use an ML model beyond the domain of the training data is in general a problem for ML, since its models, by design, essentially work by interpolating. A simple illustration of this problem is afforded in Fig. 1 superimposed with a function<sup>1</sup> learned through regression with a polynomial fit made to the data points in the interval  $(-2\pi, 2\pi)$ . In this example, the data is generated by sampling from an underlying sine

---

<sup>1</sup>The trial form for the ML algorithm (polynomial regression with features  $\{t^n | n \in \{0, 1, \dots, 6\}\}$ ) is admittedly a poor function for this. It is used only to make a point by creating a generic figure for this point.

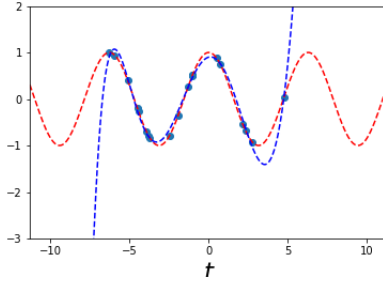


**Figure 1:** Extrapolation from fitting a polynomial to a few points from a sinusoid. The original function is shown in light grey. Notice how outside the domain where training data was available (i.e., the interval  $(-2\pi, 2\pi)$ ), the polynomial fit diverges from the true function.

curve, but the polynomial fit to it can't/doesn't assume this knowledge. Instead, it makes an excellent fit to the data in the domain of the given (training) data, but it would be ill-advised to use the model outside this interval.

To overcome this problem and be able to extrapolate a model beyond the training data for dynamical systems, the dynamics are instead viewed with respect to its phase space. For systems with no explicit time dependence, the training data will exist in this space, and not have an additional time axis. For example, the phase space plot for a system such as a harmonic oscillator would reveal a time-parametrized orbit. Fig. 2 depicts such an orbit, illustrating how the current values of  $(u, \dot{u})$  get updated by  $(\Delta u, \Delta \dot{u})$  after the time increases from  $t$  to  $t + \epsilon$ . These changes are simply defined as

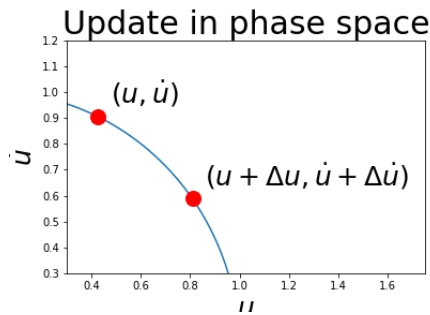


**Figure 2:** Points in phase space at  $t$  and  $t + \epsilon$ .

$$\Delta u = u(t + \epsilon) - u(t) \tag{2}$$

$$\Delta \dot{u} = \dot{u}(t + \epsilon) - \dot{u}(t) \tag{3}$$

In this approach, the challenge is how to model these updates as a function of  $(u, \dot{u})$ . Two separate models will be used:  $h_1$  and  $h_2$ ; they are referred to collectively as

$$h = (h_1, h_2).$$

$$\Delta u = h_1(u, \dot{u}) \quad (4a)$$

$$\Delta \dot{u} = h_2(u, \dot{u}) \quad (4b)$$

(Note that in these equations,  $u$  and  $\dot{u}$  are measured at  $t$ .) More generally, the model  $h$  will relate <sup>2</sup> the set of predictor variables  $X$  to the response variables  $Y$  via  $Y = h(X)$ . In this example,  $X = \{u, \dot{u}\}$  and  $Y = \{\Delta u, \Delta \dot{u}\}$ . At this point, any relevant ML technique to learn  $h$  can be used, from NNs to a regression model. When that has been accomplished, the remaining challenge is to perform the extrapolation, which is easily done via an algorithm such as Algo. 1 This will be called a *generative* algorithm, since

---

**Algorithm 1** : Generation step

---

```

Init:  $u = u(t_0)$ 
Init:  $\dot{u} = \dot{u}(t_0)$ 
for  $i = 0$  to  $N$  do
   $\text{tmp\_}h_1 = h_1(u, \dot{u})$ 
   $\text{tmp\_}h_2 = h_2(u, \dot{u})$ 
   $u \leftarrow u + \text{tmp\_}h_1$ 
   $\dot{u} \leftarrow \dot{u} + \text{tmp\_}h_2$ 
   $t \leftarrow t + \epsilon$ 
   $\text{print}(u, t)$ 
end for

```

---

it generates  $u(t)$  from the learned ML model  $h$ . It's important that the same time step ( $\epsilon$ ) that is used in the data collection also be used in the generative step; this is because the models will in general be nonlinear functions of it. Also, this algorithm as explain here is only for 2nd order order, non-driven systems. However, it can be easily extended to those cases by using additional `tmp_` variables.

### 2.3 Jet Space

For systems described by a second order DE, the phase space is just  $(u, \dot{u})$ . For systems described by a higher order DE, higher derivatives of  $u$  are needed, and thus the need for the associated jet space [Olver, 1993, Hydon, 2000] becomes apparent. Suppose the underlying space of the system is  $Q \times U$ , where  $Q$  ( $U$ ) represents the set of independent (dependent) variables. Now define  $U^{(n)}$ , the  $n$ th order prolongation of  $U$ , as the set of all possible derivatives of variables in  $U$  with respect to variables in  $Q$ , up to the  $n$ th order. Thus, the  $n$ th order jet space of  $Q \times U$  is  $\mathcal{J}^{(n)} = Q \times U^{(n)}$ .

As an example, taking  $U = \{u\}$  and  $Q = \{x, t\}$ , the second prolongation <sup>3</sup> of  $U$  is  $U^{(2)} = (u; u_x, u_t; u_{xx}, u_{xt}, u_{tt})$ , as its 2nd order jet space is  $\mathcal{J}^{(2)} = (x, t) \times U^{(2)}$ .

---

<sup>2</sup>Different models and even different predictor variables can be used when modeling each member of  $Y$ .

<sup>3</sup>The notation here is as usual:  $u_x = \partial u / \partial x$ ,  $u_{xx} = \partial^2 u / \partial x^2$ , etc.

## 2.4 Variable Choice

In picking what initial set of feature to use in modeling, the common choice is the convenient assumption of a low-complexity model that is polynomial in the variable of interest, perhaps including derivatives of that variable. If there are any special symmetry considerations, such as with a pendulum (which requires the angle to be periodic in  $2\pi$ ), that should also be included.

However, as is demonstrated in Appendix A, it's not just this initial set of features that should be included in the modeling step, but also potentially all possible products involving powers and derivatives of the original set of features. As shown in that appendix, the FJet method can be directly compared to what results from a numerical integration (such as Runge-Kutta) after it is expanded with respect to the time step.

As a guide to the reader, one can consider the following rule as a means to making sure all possible terms have been considered: If  $\mathcal{F}$  is the original set of features, then the full set of *potential* features would be

$$\mathcal{F} \rightarrow \sum_{n=0} (\mathcal{F} + \nabla_J \mathcal{F} + \nabla_J \nabla_J \mathcal{F} + \dots)^n \quad (5)$$

where  $\nabla_J$  includes all possible derivatives and  $J$  denotes any of the jet space variables being used. For example, in the case of the pendulum <sup>4</sup>, (Whether every possible combination actually appears depends on the amount of nonlinearity in the underlying DE. In particular, problems like the harmonic oscillator have no contributions beyond the first derivative.) This rubric is motivated by the expansion that results from the Runge-Kutta algorithm, and will be illustrated in the examples to follow.

## 2.5 Model choice

The model (cf. Eqs. 4) can be anything, from a neural set, to a decision tree, to a linear regression model. However, it will be especially convenient when deriving the underlying DE, as well as deriving constants of motion, that a model  $h$  take the following form

$$h(X) = a_0 f_0 + a_1 f_1 + a_2 f_2 + \dots \quad (6)$$

where the  $a_i$  are scalars and the  $f_i$  are functions of  $X$  and are called "features". Typically these features will be low-order monomials, possibly with trigonometric factors. The features will be local functions, but may in principle may include non-local terms as well. In this paper this type of model will be called *feature regression*, but it goes by other names in other papers. For example, in ML/Stats it is called functionally additive models (FAMs); in earlier work on extracting models from data, some were calling it *linear in the parameter model* [Aguirre and Letellier, 2009]. More recently, it is sometimes called *symbolic regression* by some in the ML community.

Modeling in this paper will attempt to place additional complexity into the initial input features, thereby lessening the need for complexity in the remaining part of the

---

<sup>4</sup>Using the notation of the previous section, when there is no explicit dependence on independent variables,  $\mathcal{J} = U$ , as with the harmonic oscillator and pendulum. However, when such dependencies do exist, as with the Duffing oscillator, then  $\mathcal{J} = Q \times U$ .

model. It is claimed here that this may be a general principle, that the sum of the complexity of the initial features and the complexity of the remaining part of the model is roughly constant; this would be true across different models with similar performance.

## 2.6 Constants of Motion

A DE can be defined by the hypersurface  $\mathcal{D}(x, u, u^{(1)}, \dots, u^{(n)}) = 0$ , which is defined in the jet space of this equation; here  $x$  represents the independent variables,  $u$  the dependent variables, and  $u^{(n)}$  the  $n$ th order derivative of  $u$  wrt  $x$ . A Lie symmetry  $X$  of this DE is defined as infinitesimal generators [Olver, 1993, Bluman and Kumei, 1989, Hydon, 2000] on this jet space which leads to updates of these variables which still satisfy the DE. If  $X$  is expressed as a flow in this space, such as

$$X = \xi \frac{\partial}{\partial x} + \eta \frac{\partial}{\partial u} + \eta^{(1)} \frac{\partial}{\partial u^{(1)}} + \dots \quad (7)$$

where  $\eta^{(n)}$  is the  $n$ th prolongation of  $\eta$ , the symmetry is expressed as  $X\mathcal{D} = 0$ . An invariant  $\mathcal{I}$  of this symmetry will satisfy  $X\mathcal{I} = 0$ , and so it can be solved for using the method of characteristics:

$$\frac{dx}{\xi} = \frac{du}{\eta} = \frac{du^{(1)}}{\eta^{(1)}} + \dots \quad (8)$$

For example, using the equation for  $\eta$  and  $\eta^{(1)}$ , an invariant would appear as a constant of integration ( $r$ ):

$$r = - \int^u \frac{du}{\eta} + \int^{u^{(1)}} \frac{du^{(1)}}{\eta^{(1)}} \quad (9)$$

which might instead be solved for as

$$r = - \int^u du \eta^{(1)} + \int^{u^{(1)}} du^{(1)} \eta \quad (10)$$

Also, since a function of a constant is still a constant, various transformations of  $r$  may be made for convenience. Finally, it is noted that Lie symmetries are normally obtained to identify families of solutions, while here the focus will be on the time evolution of a single solution representing a symmetry.

In the above expressions,  $r$  is the constant of motion from an indefinite integral. However, in the more numerical setting of an ML application where analytical expressions for  $\eta$  and  $\eta^{(1)}$  are unavailable, a different approach is needed. In that case, one might instead compute the change in  $r$  as  $\delta r$ , computed as a *definite* integral along the trajectory  $\Gamma$ :

$$\delta r = - \int_{\Gamma} du \eta^{(1)} + \int_{\Gamma} du^{(1)} \eta \quad (11)$$

In this approach,  $\delta r$  is zero (by definition), and thus what one hopes to gain is an understanding of the various contributions to it.

## 2.7 Summary

The logical development of this section can be traced as follows. The initial problem with modeling the dynamics is that it is usually done on a graph of the variable versus time (e.g.,  $u$  vs.  $t$ ). Since the training data necessarily has a limited domain, extrapolating to times beyond that is problematic. To get around that, the problem is instead considered in the phase (e.g.,  $u, \dot{u}$ ). However, that creates the problem of how to capture the dynamics. The issue is solved by determining the (FJet) mapping of  $u, \dot{u}$  variables in this phase space. The choice of variables for the model is inspired by the jet space of the underlying DEs. After that, it was a simple matter to recover  $u(t)$  via the generative algorithm given in Algo. 1.

The next step is to find a good model for this mapping. It is suggested to consider "feature regression", since it is straightforward, can be compared to RK, and also makes it easy to later determine the underlying DE. If in addition it's possible to obtain training data for different settings of various parameters, then it becomes possible to determine the underlying DE with functional dependences on those parameters.

## 3 Example: Harmonic Oscillator (damped)

The equation for a harmonic oscillator is relevant for a myriad of physical systems<sup>5</sup>, perhaps most well known being the small angle limit of a pendulum. Here,  $u$  represents the deviation from the minimum, and  $\omega_0$  its natural frequency:

$$\ddot{u} + 2\gamma\dot{u} + \omega_0^2 u = 0, \quad (12)$$

Its general solution in the underdamped case is  $u = Ae^{-\gamma t} \cos(\omega t + \alpha)$ , where  $\omega = \sqrt{\omega_0^2 - \gamma^2}$ ,  $A$  is the amplitude, and  $\alpha$  is the phase. This section will mostly consider the case of  $\gamma \neq 0$ , except where stated otherwise.

### Training Data

For the present example, training data was generated from 2000 random samples<sup>6</sup>, using  $\omega = 1$ ,  $t \in (0, 2T)$ ,  $u \in (-2, 2)$ ,  $\dot{u} \in (-2, 2)$ . Data point pairs were created using a randomly sampled point, with a new point being created via a single step of a 4th-order Runge-Kutta scheme; the time step was  $dt = 0.1$ . In the plots in Fig. 3, only the first of each pair is plotted, since the points are so close to each other. In the figures, the color of the points is determined by the sign of  $\Delta u$  or  $\Delta \dot{u}$ : it is red (blue) if the sign is positive (negative). Also, the size of the dots are proportional to the magnitude of  $\Delta u$  (or  $\Delta \dot{u}$ ); the same scaling was used for both plots in the figure. With a keen eye<sup>7</sup>, the reader may notice that the blue/red regions do not separate perfectly along the

<sup>5</sup>Indeed, any system that has oscillations about some stable point can be described by a multivariate harmonic oscillator.

<sup>6</sup>Far fewer were needed to get a good fit. This was used in order to be able to see clearly that the separation line between red/blue wasn't perfectly horiz or vertical.

<sup>7</sup>2000 points were used for these plots, so the reader could more easily see the slight tilt in the red/blue boundaries. Far fewer points were needed for the modeling to follow.

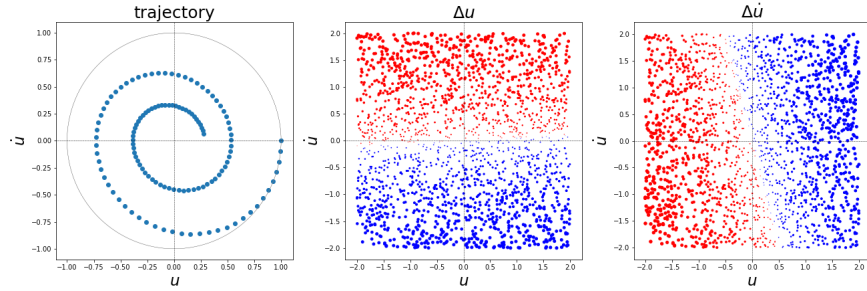


**Figure 3:** The left plot corresponds to the (clockwise) path taken by updates of the system, starting from an initial condition of  $(u, \dot{u}) = (1, 0)$ . The light gray circle is added as a visual reference, and corresponds to the path that would have been taken in the undamped case. The center and right plots correspond to the changes in  $u$  and  $\dot{u}$ , as defined in Eq. 3. The dot sizes are proportional to the magnitude of what is being plotted, and is red (blue) for positive (negative) values.

axes (i.e., the horizontal axis for  $\Delta u$ , and the vertical axis for  $\Delta \dot{u}$ ). This is an artifact of the discretization, and is discussed more fully in Appendix A. These figures (especially the one on the right) give us the important information that they may be modeled as a unique function of  $u$  and  $\dot{u}$ . The plots reveal that both  $\Delta u$  and  $\Delta \dot{u}$  vary smoothly in the  $(u, \dot{u})$  plane. Importantly, it appears that there are no "high variance" regions. Such regions would have, for example, a co-location of red and blue dots, or of dots of markedly different sizes. Either of those could be detected numerically by measuring the variance (of  $\Delta u$  or  $\Delta \dot{u}$ ) as a function of  $(u, \dot{u})$ .

## Model

Given these observations, it appears that it would suffice from a modeling perspective to simply have  $h_1$  and  $h_2$  be linear combinations of  $u$  and  $\dot{u}$ . Recalling Eq. 4,  $h_1$  and  $h_2$  model the values  $\Delta u$  and  $\Delta \dot{u}$ . In the interest of generality, and with insights from Appendix A, the modeling is begun with the allowance for an augmented set of potential predictors

$$\{u, \dot{u}\} \rightarrow \{1, u, \dot{u}, t, t^2, u^2, u\dot{u}, \dots\}$$

where "1" indicates a constant term<sup>8</sup>.

The elements in this new set may now be taken as input features into an appropriate ML model. As already discussed, while many ML models can be used (such as a NN), it is convenient here to use *feature regression*, since it will facilitate determining the underlying DE. After following the usual steps in regression<sup>9</sup>, the resulting response

<sup>8</sup>Expect no constant term, since it appears the dot size is zero near the origin, in both plots in Fig. 3. Also, note that if  $\dot{u}$  were included in the predictors, a collinearity would manifest itself, a signal to the developer that it should be removed.

<sup>9</sup>The only variables now considered are those that made a significant contribution (in terms of size and p-value)

( $Y$ ) and predictor ( $X$ ) variables are chosen to be

$$Y = (\Delta u, \Delta \dot{u})^T \quad (13)$$

$$X = (u, \dot{u})^T \quad (14)$$

and the feature regression model  $h(X)$  appears as a matrix-vector product,

$$Y = \epsilon \begin{bmatrix} a_1 & a_2 \\ b_1 & b_2 \end{bmatrix} X \quad (15)$$

In this approach, one can now determine the coefficients  $a_i$  and  $b_i$  ( $i = 1, 2$ ) using only regression. Using the time step  $\epsilon = 0.1$ , the resulting values for these coefficients are shown in the center column in Table 1. In the feature regression modeling, regularization

	$\epsilon = 0.1$	$\epsilon \rightarrow 0$
$a_1$	-0.050	0
$a_2$	0.988	1
$b_1$	-0.988	-1
$b_2$	-0.247	-0.2

**Table 1:** In the center column are values of the coefficients when  $\epsilon = 0.1$ . The right column contains those same values after extrapolating to  $\epsilon \rightarrow 0$ , and are derived in the next section.

was not used, in contrast to approaches by other authors [eg. Crutchfield and McNamara, 1987, Rudy et al., 2017]. For example, one might have used Elastic Net regularization to drive small, less important coefficients down to zero, enabling an easier identification of a "minimal model". Instead, the  $\epsilon$ -dependence of these parameters will be studied, to determine their behavior as  $\epsilon \rightarrow 0$  and ascertain the underlying DE. However, if one is not interested in this limit, it would make sense to use regularization.

## Underlying DE

Next, the values for these coefficients are found in the limiting case of  $\epsilon \rightarrow 0$ , using the same approach as in the previous examples. Graphs for the behavior of these coefficients are shown in Fig. 4. The data was based on fitting these coefficients with a mapping using values for  $\epsilon$  from 0.1 to 0.001. Upon extrapolating a polynomial fit of these plots to  $\epsilon = 0$ , the values in the rightmost column of Table 3 resulted. Deviations in these values due to the fit were on the order of  $10^{-15}$  to  $10^{-18}$ . The mapping of Eq. 15 may now be rewritten in this limiting case, and the variables will be written using the standard differential notation (ie,  $\epsilon \rightarrow dt$ ,  $\Delta u \rightarrow du$ ,  $\Delta \dot{u} \rightarrow d\dot{u}$ ), producing

$$du = dt[\dot{u}] \quad (16a)$$

$$d\dot{u} = dt[-0.2\dot{u} - u] \quad (16b)$$

The first of these equations (Eq. 16a) is just a contact condition, and reflects the fact that in the space  $(u, \dot{u})$ , not all three quantities  $du$ ,  $dt$ ,  $\dot{u}$  are independent (i.e.,  $\dot{u} = du/dt$ )

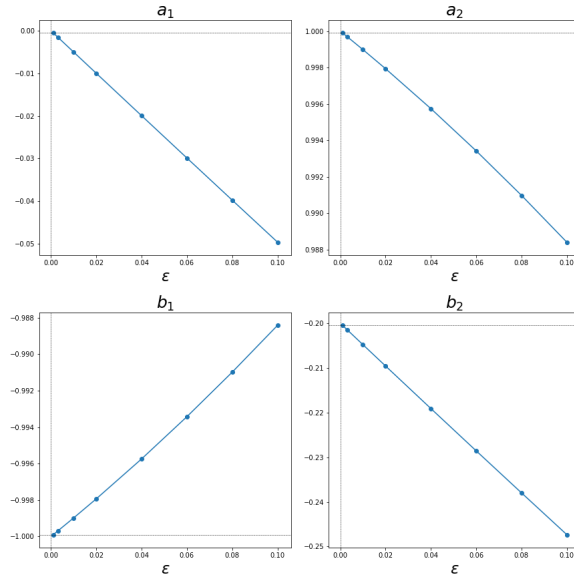


**Figure 4:** Plots of the  $\epsilon$ -dependence of the  $a_i$  coefficients ( $i = 1, 2$ ) in the model  $h(X)$  (cf. Eq. 15). The values obtained by extrapolating these curves to  $\epsilon = 0$  are listed in Table 1.

<sup>10</sup>. The second of these equations (Eq. 16b) is just equivalent to the original equation of motion for the pendulum (Eq. 12), with the chosen parameter values ( $\omega_0 = 1$  and  $\gamma = 0.1$ ).

### 3.1 Parameter Dependence

What was obtained in the previous section is the equation of motion based on the choice  $\omega_0 = 1$ ,  $\gamma = 0.1$ . In this section, the actual functional dependence on  $\omega_0$  and  $\gamma$  within the equation of motion is deduced.

The idea here is to consider a given value of  $\epsilon$ , and several values of  $\omega_0$ . This produces a plot versus  $\omega_0$ , which is then fit with a low-order polynomial in  $\omega_0$ . Thus, the fitting parameters are now determined for that one, given value of  $\epsilon$ . Next, this procedure is repeated for several other small values of  $\epsilon$ , and the result is extrapolated to  $\epsilon = 0$ . The results differed from the expected exact values only on the order of machine precision (about  $10^{-15}$ ).

$$b_1 = -\omega_0^2 + \dots \quad (17)$$

$$b_2 = -2\gamma + \dots \quad (18)$$

Shown in Fig. 5 is the  $\omega_0$  and  $\gamma$  dependence for these parameters in the specific case of  $\epsilon = 0.001$ , where the data is seen to follow the functional form of a quadratic (the

<sup>10</sup>Of course, this is a slight abuse of notation, since derivatives are defined in a limiting procedure.

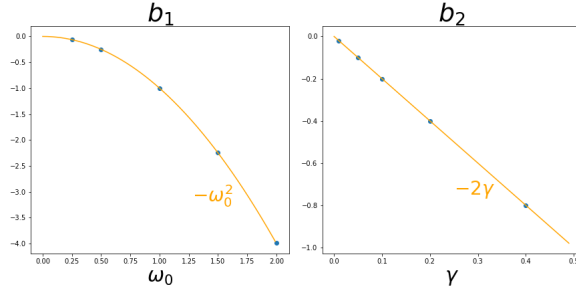


**Figure 5:** Comments... as a visual guide, the exact curves for  $\omega_0^2$  and  $-2\gamma$  are added to the left and right plots, respectively.

exact quadratic curve is drawn in yellow, as a visual guide). From this, now know that Eq. 16a and Eq. 16b can be replaced with

$$du = dt[\dot{u}] \tag{19}$$

$$d\dot{u} = dt[-\omega_0^2 u - 2\gamma \dot{u}] \tag{20}$$

from which the original equation of motion (Eq. 12) immediately follows. In summary, it has been shown how to obtain the complete equation of motion (along with parameter dependence), from data.

### Extrapolation & Stability

The ability of this model to extrapolate beyond the original training data can also be demonstrated. Using the model parameter values found using  $\epsilon = 0.1$  (i.e, the center column in Table 1), and following the rubric of the generative algorithm (Algo. 1), Fig. 6 results.

The stability is assessed in the case  $\omega_0 = 1, \gamma = 0$ , so that it can easily be compared to a known theoretical solution for the decay of the energy [Young, 2020], which is expressed as

$$E_n/E_0 = \exp(\lambda n) \tag{21}$$

at the  $n$ th iteration. Thus, a  $\lambda$  closer to 0 means it is more stable. Computing  $E_n$  for all cases and determining  $\lambda$  from that led to the values in Table 2 The most obvious aspect to this table is that  $\lambda$  is about  $10^9$  times smaller than the  $\lambda$  for RK4, which means it remains stable for about  $10^9$  times longer as with RK4. These values agree extremely well with an analytical solution in Appendix C.

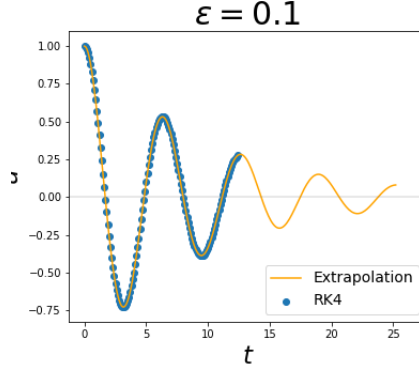


**Figure 6:** A comparison of the extrapolation of FJet to data generated by RK2, over the time range used for the training data  $(0, 2T)$ , where  $T = 2\pi/\omega_0$ .

scheme	$\lambda$
Euler	$9.94 \times 10^{-2}$
RK2	$2.49 \times 10^{-5}$
RK4	$-1.38 \times 10^{-8}$
FJet	$-1.63 \times 10^{-17}$

**Table 2:** Note that (in the undamped case) FJet remains stable about  $10^9$  times longer than RK4 in this example. A simulation was run for 10,000 iterations, with the initial condition of  $(u, \dot{u}) = (1, 0)$ . These results were computed for the  $\gamma = 0$  case.

### 3.2 Constants of Motion

It has been shown how to model the data for  $\Delta u$  and  $\Delta \dot{u}$ , and to determine the parameter dependencies in the small- $\epsilon$  limit, which yields

$$\begin{bmatrix} h_1 \\ h_2 \end{bmatrix} = \begin{bmatrix} 0 & 1 \\ -\omega_0^2 & -2\gamma \end{bmatrix} \begin{bmatrix} u \\ \dot{u} \end{bmatrix} \epsilon \quad (22)$$

By considering these updates through the lens of Lie symmetries applied to a DE, one can identify that for a change in the independent variable (time) by the amount  $\epsilon$  there is an associated change in  $u$  and  $\dot{u}$  with

$$\eta = h_1/\epsilon \quad (23)$$

$$\eta^{(1)} = h_2/\epsilon \quad (24)$$

The next step is to use these expressions for  $\eta$  and  $\eta^{(1)}$  in Eqn. 8 to determine  $r$  (or a convenient function of  $r$ ), as discussed in Sec. 2.6

A direct integration of Eqn. 8 using the expressions for  $\eta$  and  $\eta^{(1)}$  in Eqn. 22 leads

to

$$r = \frac{1}{2}(\omega_0^2 u^2 + \dot{u}^2) + 2\gamma \int \dot{u} du \quad (25)$$

The first two terms on the RHS are the energy (using  $m = 1$  in Eq. 12), and the third term is the dissipation; it should be recognizable as the force ( $2\gamma\dot{u}$ ) integrated over the distance  $u$ . In Fig. 7 these two quantities are computed along a trajectory for a single initial condition  $((u, \dot{u}) = (1, 0))$ , along with their sum ( $r$ ). What is noticeable is that

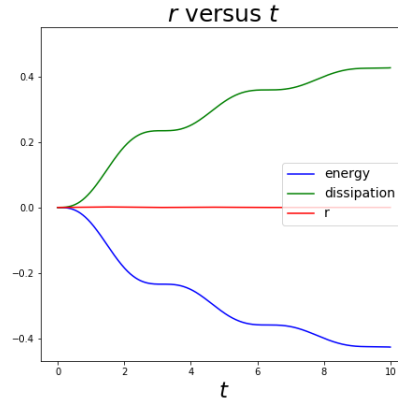


**Figure 7:** Using the initial conditions  $(u, \dot{u}) = (1, 0)$ , and computing the change in energy and energy lost to dissipation along a trajectory as a function of time in the damped case ( $\gamma = 0.1$ ). Note that the sum of these contributions ( $\delta r$ ) is constant.

the  $r$  is constant (as required). Thus the loss in the energy can be identified with the work done by the dissipation. In contrast, in a physics context the only constants of motion normally found are conserved quantities, such as the energy or momentum, for example. In this case, the conserved quantity  $r$  corresponds to the energy (or a function thereof) of the larger system (including  $u(t)$  and the dissipation). However, it is emphasized that  $r$  is not in general related to such a physical concept. Finally, the computation which produced this graph is based on a single trajectory. Next, the constant  $r$  will be computed for all values in the  $(u, \dot{u})$  plane.

### Phase Space ( $\gamma = 0$ )

The case where there is no dissipation (i.e.,  $\gamma = 0$ ) is straightforward and  $r$  is easily found (using Eqn. 11, for example)

$$r(u, \dot{u}) = \frac{1}{2} [\omega_0^2 u^2 + \dot{u}^2]$$

If this represents a physical system of a mass ( $m$ ) on a spring (with constant  $k$ ), then the energy is  $mr$ . Contour plots for this function are not shown, since they would obviously just be ellipses.

## Phase Space ( $\gamma \neq 0$ )

The case where there is dissipation (i.e.,  $\gamma \neq 0$ ) leads to qualitative changes in  $r(u, \dot{u})$ . The details of the calculation are in Appendix C, and lead to

$$r_n(u, \dot{u}) = \frac{1}{2}[\omega^2 u^2 + (\gamma u + \dot{u})^2] \exp\left(2\frac{\gamma}{\omega}\phi_n\right)$$

where

$$\begin{aligned}\tan \phi &= -(\gamma u + \dot{u})/(\omega u) \\ \phi_n &= \phi + 2n\pi\end{aligned}$$

and  $n = \dots, -2, -1, 0, 1, 2, \dots$ . This expression for the contours is unique in that it now depends on Riemannian sheets, with  $n = 0$  indicating the principal sheet. The angle  $\phi$  is computed so that its range is  $[0, 2\pi)$ ; it is measured from the branch cut.

In Fig. 8 this constant is plotted for the cases  $n = 0$  and  $n = 1$ . The dissipation

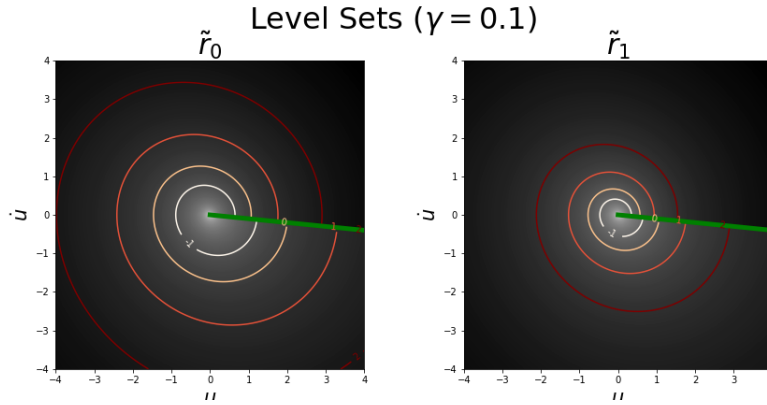


**Figure 8:** Contour plots of  $\tilde{r}_n = \log(2r_n)$ .

causes the curves to spiral inward in a clockwise fashion. The branch cut (the green line) limits the beginning and end of a trajectory. Thus when a trajectory reaches a branch cut, it jumps to the next highest sheet. The differently colored curves in each plot each have their own value; they act as level sets for this contour plot. As can be seen, the value of  $r$  is continuous except in the neighborhood of the branch cut. When crossing the branch cut from above (below), the sheet number increases (decreases). Note that these curves replace the energy contours used to characterize an undamped oscillator.

## 4 Example: Pendulum (damped)

The damped pendulum is an important extension of the harmonic oscillator from the last example, in that it introduces nonlinearities and periodicity. The equation of motion is

$$\ddot{u} + 2\gamma\dot{u} + \omega_0^2 \sin u = 0 \quad (26)$$

where  $\omega_0$  is the natural frequency in the small- $u$  limit and  $\gamma$  is the damping coefficient.

## Training Data

The parameter values  $\omega_0 = 1.0$  and  $\gamma = 0.1$  are used in Fig. 9, which includes multi-start trajectories (left plot), and update maps for  $\Delta u$  and  $\Delta \dot{u}$  (center and right plots). Note that in the left plot, the rotation is clockwise; in the upper (lower) half of the

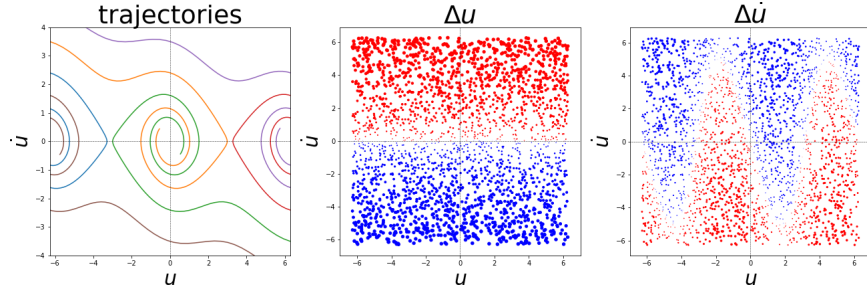


**Figure 9:** The left plot corresponds to the paths taken by updates of the system, starting from a number of different initial points. Note the  $2\pi$  periodicity along  $u$ . The center and right plots correspond to the changes in  $u$  and  $\dot{u}$ , as defined in Eq. 3. The dot sizes are proportional to the magnitude of what is being plotted, and is red (blue) for positive (negative) values.

plane, the motion is to the right (left). As discussed before, the  $\Delta$  plots were created by randomly selecting  $(u, \dot{u})$  values and then doing a single time step update (with  $\epsilon = 0.1$ ), in this case using RK2. This created a data pair, and allowed a creation of  $\Delta u$  and  $\Delta \dot{u}$ ; the red (blue) colors indicate positive (negative) values. It is these plots which will be fitted by an ML procedure, such as NNs, feature regression, random forest regressors, etc. Also, the three plots in this figure have  $u$  and  $\dot{u}$  each range over  $(-2\pi, 2\pi)$  to display the periodic structure, but in the actual training data only the range of  $(-\pi, \pi)$  was used.

## Model

As a starting assumption, based on experience with a harmonic oscillator (cf. Sec. 3), one might begin by considering the feature set  $\{u, \dot{u}\}$ . However, the domain knowledge in this case is that  $u$  must be periodic, so instead the starting feature set under consideration is  $\{\dot{u}, \cos u, \sin u\}$ . As discussed in Sec. 2.4, numerical integration techniques (cf. Appendix A) suggest one should use a larger feature set, such as

$$\{\dot{u}, \cos u, \sin u\} \rightarrow \{\dot{u}, \cos u, \sin u, \dot{u} \cos u, \dot{u} \sin u, \dots\}$$

The elements in this new set may now be taken as input features into an appropriate ML model. As already discussed, while many ML models can be used (such as a NN), it is convenient here to use *feature regression*, since it will facilitate determining the

underlying DE. After following the usual steps in regression <sup>11</sup>, the resulting response ( $Y$ ) and predictor ( $X$ ) variables are chosen to be

$$Y = (\Delta u, \Delta \dot{u})^T \quad (27)$$

$$X = (\dot{u}, \sin u, \dot{u} \cos u)^T \quad (28)$$

and the feature regression model  $h(X)$  appears as a matrix-vector product,

$$Y = \epsilon \begin{bmatrix} a_1 & a_2 & a_3 \\ b_1 & b_2 & b_3 \end{bmatrix} X \quad (29)$$

In this approach, one can now determine the coefficients  $a_i$  and  $b_i$  ( $i = 1, 2, 3$ ) using only regression. Using the time step  $\epsilon = 0.1$ , the resulting values for these coefficients are shown in the center column in Table 3. In the feature regression modeling, regularization

	$\epsilon = 0.1$	$\epsilon \rightarrow 0$
$a_1$	0.990	1
$a_2$	-0.049	0
$a_3$	0	0
$b_1$	-0.197	-0.2
$b_2$	-0.985	-1
$b_3$	-0.049	0

**Table 3:** In the center column are values of the coefficients when  $\epsilon = 0.1$ . The right column contains those same values after extrapolating to  $\epsilon \rightarrow 0$ , and are derived in the next section.

was not used, in contrast to approaches by other authors [eg. Crutchfield and McNamara, 1987, Rudy et al., 2017]. For example, one might have used elastic net regularization Hastie et al. [2009] to drive small, less important coefficients down to zero, enabling an easier identification of a "minimal model". Instead, the  $\epsilon$ -dependence of these parameters will be studied, to determine their behavior as  $\epsilon \rightarrow 0$  and ascertain the underlying DE. However, if one is not interested in this limit, it would make sense to use regularization.

## Underlying DE

Next, the values for these coefficients are found in the limiting case of  $\epsilon \rightarrow 0$ , using the same approach as in the previous examples. Graphs for the behavior of these coefficients are shown in Figs. 10, 11. The data was based on fitting these coefficients with a mapping using values for  $\epsilon$  from 0.1 to 0.001. Upon extrapolating a polynomial fit of these plots to  $\epsilon = 0$ , the values in the rightmost column of Table 3 resulted. The mapping of Eq. 29 may now be rewritten in this limiting case, and the variables will

<sup>11</sup>The only variables now considered are those that made a significant contribution (in terms of size and p-value)

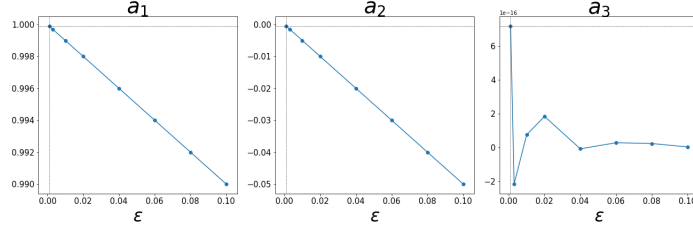


**Figure 10:** Plots of the  $\epsilon$ -dependence of the  $a_i$  coefficients ( $i = 1, 2, 3$ ) in the model  $h(X)$  (cf. Eq. 29).

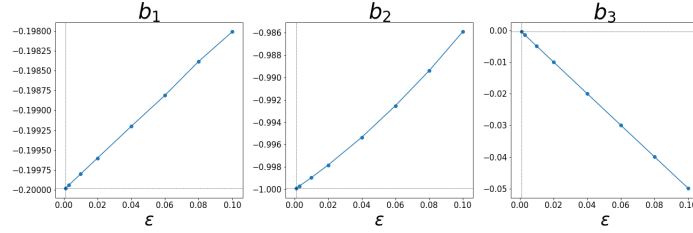


**Figure 11:** Plots of the  $\epsilon$ -dependence of the  $b_i$  coefficients ( $i = 1, 2, 3$ ) in the model  $h(X)$  (cf. Eq. 29).

be written using the standard differential notation (ie,  $\epsilon \rightarrow dt$ ,  $\Delta u \rightarrow du$ ,  $\Delta \dot{u} \rightarrow d\dot{u}$ ), producing

$$du = dt[\dot{u}] \tag{30a}$$

$$d\dot{u} = dt[-0.2\dot{u} - \sin u] \tag{30b}$$

The first of these equations (Eq. 30a) is just a contact condition, and reflects the fact that in the space  $(u, \dot{u})$ , not all three quantities  $du$ ,  $dt$ ,  $\dot{u}$  are independent (i.e.,  $\dot{u} = du/dt$ )<sup>12</sup>. The second of these equations (Eq. 30b) is just equivalent to the original equation of motion for the pendulum (Eq. 26), with the chosen parameter values.

## Extrapolation & Stability

The ability of this model to extrapolate beyond the original training data can also be demonstrated. Using the model parameter values found in the undamped case ( $\gamma = 0$ ), using  $\epsilon = 0.1$  (i.e, the center column in Table 3), and following the rubric of the generative algorithm (Algo. 1), Fig. 12 results. In addition, the stability can be assessed by a long time comparison between the extrapolation of FJet and RK2 in Fig. 13, by examining the energy (left plot), the absolute value of the difference between the solutions (center plot), and a short-time examination of how a phase difference develops between the two (right plot). The energy is computed as

<sup>12</sup>Of course, this is a slight abuse of notation, since derivatives are defined in a limiting procedure.

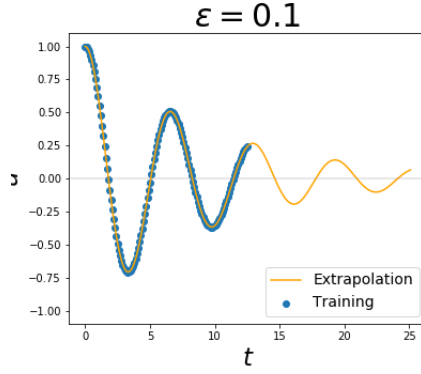


**Figure 12:** A comparison of the extrapolation of FJet to data generated by RK2 in the damped case ( $\gamma = 0.1$ ), over the time range used for the training data  $(0, 2T)$ , where  $T = 2\pi/\omega_0$ .

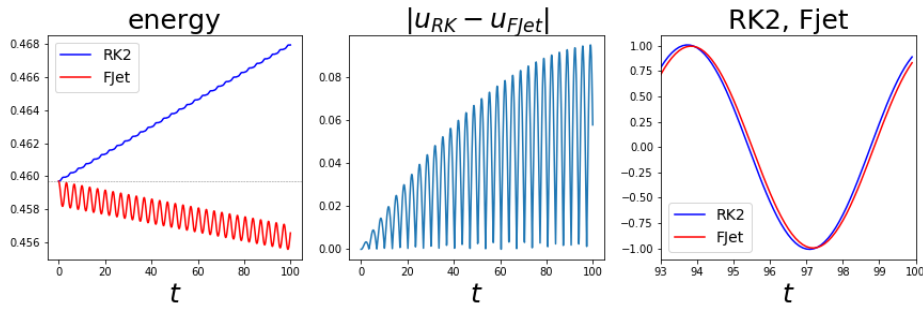


**Figure 13:** Three plots indicating the difference between the extrapolation from FJet and RK2 in the undamped case ( $\gamma = 0$ ). The left plot compares the energy for each, using Eq. 31. The center plot is of the absolute value of the difference between the two solutions, plotted as a function of time. The right plot compares the two solutions, after about 15 periods.

$$E = \frac{1}{2}\dot{u}^2 + \omega_0^2(1 - \cos u) \quad (31)$$

and is shown as a faint gray line in the left plot. Since the initial condition is  $(u, \dot{u}) = (1, 0)$ , the energy is  $1 - \cos(1) \approx 0.46$ .

### Constants of Motion

Again interpreting  $h_1/\epsilon$  as  $\eta$ , and  $h_2/\epsilon$  as  $\eta^{(1)}$  in the  $\epsilon \rightarrow 0$  limit of the feature regression model, it follows

$$\begin{bmatrix} \eta \\ \eta^{(1)} \end{bmatrix} = \begin{bmatrix} 0 & 1 \\ -\omega_0^2 & -2\gamma \end{bmatrix} \begin{bmatrix} \sin u \\ \dot{u} \end{bmatrix} \quad (32)$$

Following Sec. 2.6, the constant of motion from integration results in

$$\delta r(t) = - \int_{\Gamma} du \eta^{(1)} + \int_{\Gamma} d\dot{u} \eta \quad (33)$$

$$= \delta E + w_{diss} \quad (34)$$

where

$$\delta E = \omega_0^2 \int_{\Gamma} du \sin u + \int_{\Gamma} d\dot{u} \dot{u} \quad (35)$$

$$w_{diss} = 2\gamma \int_{\Gamma} du \dot{u} \quad (36)$$

are computed along the trajectory  $\Gamma(t)$  from  $(u(0), \dot{u}(0))$  to  $(u(t), \dot{u}(t))$ . Here,  $\delta E$  is the change in energy, and  $w_{diss}$  is the energy lost through dissipation (i.e., because of the damping force). Integrating these quantities along a path in phase space (with initial condition  $((u, \dot{u}) = (1, 0))$  yields Fig. 14. Once again, it is shown that  $\delta r$  is a

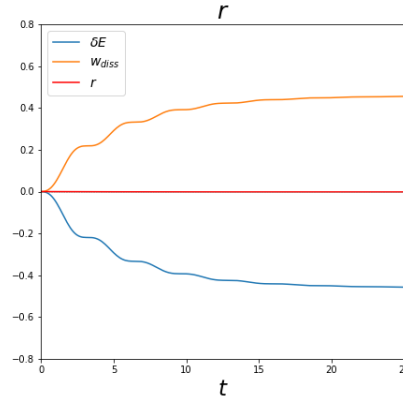


**Figure 14:** Using the initial conditions  $(u, \dot{u}) = (1, 0)$ , and computing the change in energy and energy lost to dissipation along a trajectory as a function of time in the damped case ( $\gamma = 0.1$ ). Note that the sum of these contributions ( $\delta r$ ) is constant.

constant. Also,  $\delta r$  may again be interpreted as the change of the energy of the system and environment, which is zero; it is expressed here, since  $\delta r = 0$ , as  $\delta E = -w_{diss}$ . However, the reader is cautioned that this is not a general feature of this Lie symmetry technique, which doesn't require a physical context. Finally, note that if  $\gamma = 0$ , the integration could easily be done, reproducing the expression for the energy given in Eq. 31.

## 5 Example: Duffing Oscillator

The Duffing oscillator [Duffing, 1918, Moon and Holmes, 1979, Jackson, 1991] is based on the damped oscillator seen in Sec. 3, except it is augmented by a nonlinear restoring

term (proportional to  $\beta$ ) and a force  $p(t)$ , and  $\alpha$  is allowed to be negative. It appears here as

$$\ddot{u} + 2\gamma\dot{u} + \alpha u + \beta u^3 = p(t) \quad (37a)$$

$$p(t) = A \sin \Omega t \quad (37b)$$

## Training Data

Throughout this example, unless specified otherwise, the parameter values will be:  $\gamma = 0.15$ ,  $\alpha = -1$ ,  $\beta = 1$ ,  $A = 0.28$ , and  $\Omega = 1.2$ . These values are used to create Fig. 15. The left plot was created from a single run with initial condition  $(u, \dot{u}) = (1, 0)$ ;

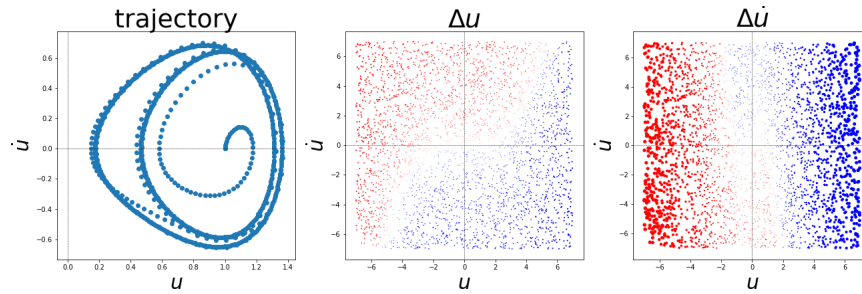


**Figure 15:** The left plot corresponds to the paths taken by updates of the system, starting from a number of different initial points. Note that the orbit is in the period-2 phase. The center and right plots correspond to the changes in  $u$  and  $\dot{u}$ , as defined in Eq. 3. The dot sizes are proportional to the magnitude of what is being plotted, and is red (blue) for positive (negative) values. Also, note the different scale of the left plot compared to the center and right plots.

the updates are in a clockwise rotation and reveal a period-2 oscillation. The center and right plots are update maps for  $\Delta u$  and  $\Delta \dot{u}$ . The first step in creating the training data was to randomly sample  $(u, \dot{u}, t)$ ; the random time was inserted into Eq. 37b to create sampling for  $p$  and  $\dot{p}$ . The second step was to then do a single time step update with RK2 using  $\epsilon = 0.1$ . This created a data pair, and allowed a creation of  $\Delta u$  and  $\Delta \dot{u}$ .

With a keen eye, the reader may note that in the right plot of Fig. 15 there is a slight overlap between positive (red) and negative (blue) dots. This results in a larger variance in the values and indicates that these two variables aren't sufficient to model  $\Delta u$  and  $\Delta \dot{u}$  (i.e., the set of predictor variables needs to be augmented). This occurs because the feature set  $\{u, \dot{u}\}$  is not sufficient to model  $\Delta u$  and  $\Delta \dot{u}$  with low variance. Also, in anticipation of using  $p$  and  $\dot{p}$  as predictors, those data were also collected and stored for each  $\Delta u$  and  $\Delta \dot{u}$ .

## Model

As a starting assumption, based on experience with a harmonic oscillator (cf. Sec. 3), one might begin by considering the feature set  $\{u, \dot{u}, p\}$ . However, as discussed in

Sec. 2.4, numerical integration techniques (cf. Appendix A) suggest one should use a larger feature set, such as

$$\{u, \dot{u}, p\} \rightarrow \{u, \dot{u}, u^2, u\dot{u}, \dot{u}^2, u^3, u^2\dot{u}, u\dot{u}^2, \dot{u}^3, p, \dot{p}, pu, p\dot{u}, \dot{p}u, \dot{p}\dot{u}, \dots\}$$

The elements in this new set may now be taken as input features into an appropriate ML model. As already discussed, while many ML models can be used (such as a NN), it is convenient here to use *feature regression*, since it will facilitate determining the underlying DE. After following the usual steps in regression <sup>13</sup>, the resulting response ( $Y$ ) and predictor ( $X$ ) variables are chosen to be

$$Y = (\Delta u, \Delta \dot{u})^T \quad (38)$$

$$X = (u, \dot{u}, u^3, u^2\dot{u}, u\dot{u}^2, \dot{u}^3, p, \dot{p})^T \quad (39)$$

and the feature regression model  $Y = h(X)$  appears as a matrix-vector product <sup>14</sup>,

$$Y = \epsilon \begin{bmatrix} a_1 & a_2 & a_3 & 0 & 0 & 0 & a_7 & 0 \\ b_1 & b_2 & b_3 & b_4 & b_5 & b_6 & b_7 & b_8 \end{bmatrix} X \quad (40)$$

In this approach, one can now determine the coefficients  $a_i$  and  $b_i$  ( $i = 1, \dots, 8$ ) using only regression. Using the time step  $\epsilon = 0.1$ , the resulting values for these coefficients are shown in the center column in Table 4. Note that the resulting FJet mapping can

	$\epsilon = 0.1$	$\epsilon \rightarrow 0$
$a_1$	0.0500	0
$a_2$	0.9850	1
$a_3$	-0.0499	0
$a_7$	0.0499	0
$b_1$	0.9850	1
$b_2$	-0.2455	-0.3
$b_3$	-0.985	-1
$b_4$	-0.1499	0
$b_5$	$-7.5 \times 10^{-3}$	0
$b_6$	$-1.25 \times 10^{-4}$	0
$b_7$	0.9832	1
$b_8$	0.0499	0

**Table 4:** In the center column are values of the coefficients when  $\epsilon = 0.1$ . The right column contains those same values after extrapolating to  $\epsilon \rightarrow 0$ , and are derived in the next section. The coefficients  $a_4, a_5, a_6$ , and  $a_8$  are close to zero and so are disregarded.

then make use of any forcing term to be used in the extrapolation algorithm (Algo. 1). Because of its reliance on a general  $p$  (and  $\dot{p}$ ), it resembles a Green's function approach.

<sup>13</sup>The only variables now considered are those that made a significant contribution (in terms of size and p-value)

<sup>14</sup>As it turned out, the terms  $u\dot{u}^2$  and  $\dot{u}^3$  are not part of the recommended  $X$  for RK2 (see Appendix A). In the matrix below they correspond to parameters  $b_5$  and  $b_6$ ; note that these two parameters are noticeably smaller than the others.

In the feature regression modeling, regularization was not used, in contrast to approaches by other authors [eg. Crutchfield and McNamara, 1987, Rudy et al., 2017]. For example, one might have used regularization to drive small, less important coefficients down to zero, enabling an easier identification of a "minimal model". Instead, the  $\epsilon$ -dependence of these parameters will be studied, to determine their behavior as  $\epsilon \rightarrow 0$  and ascertain the underlying DE. However, if one is not interested in this limit, it would make sense to use regularization.

## Underlying DE

Next, the values for these coefficients are found in the limiting case of  $\epsilon \rightarrow 0$ , using the same approach as in the previous examples. Graphs for the behavior of these coefficients are shown in Figs. 16, 17. The time steps used in creating these figures ranged from

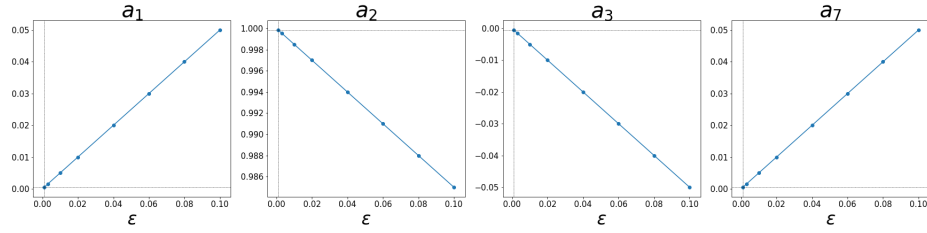


**Figure 16:** Plots of the  $\epsilon$ -dependence of the  $a_i$  coefficients ( $i = 1, 2, 3, 7$ ) in the FJet mapping matrix (cf. Eq. 40).

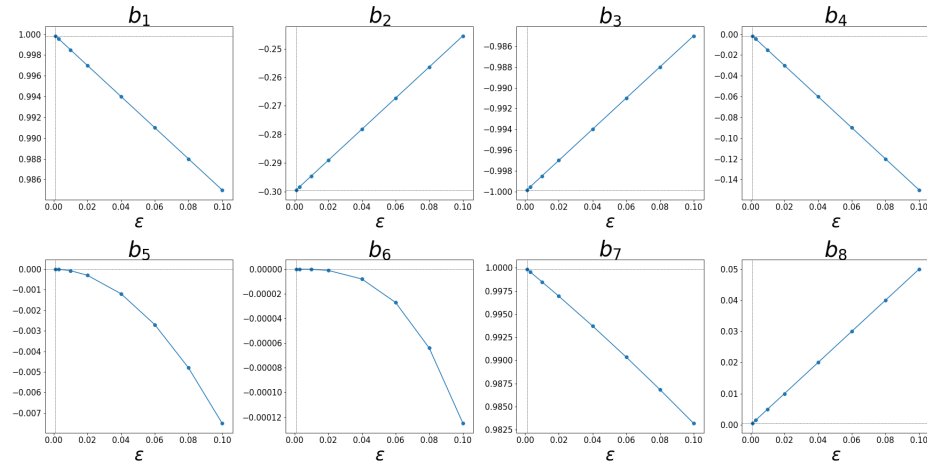


**Figure 17:** Plots of the  $\epsilon$ -dependence of the  $b_i$  coefficients ( $i = 1, 2, \dots, 8$ ) in the FJet mapping matrix (cf. Eq. 40).

0.1 to 0.001. Upon extrapolating a polynomial fit of these plots to  $\epsilon = 0$ , the values in the rightmost column of Table 4 resulted, and determine the underlying DE. With the standard differential notation (i.e.,  $\epsilon \rightarrow dt$ ,  $\Delta u \rightarrow du$ ,  $\Delta \dot{u} \rightarrow d\dot{u}$ ), the mapping produces

$$du = dt[\dot{u}] \quad (41a)$$

$$d\dot{u} = dt[u - 0.3\dot{u} - u^3 + p(t)] \quad (41b)$$

The first of these equations (Eq. 30a) is just a contact condition, and reflects the fact that in the space  $(u, \dot{u})$ , not all three quantities  $du$ ,  $dt$ ,  $\dot{u}$  are independent (i.e.,  $\dot{u} = du/dt$ )<sup>15</sup>. The second of these equations (Eq. 30b) is just equivalent to the original equation of motion for the Duffing oscillator (Eq. 37a), with the chosen parameter values.

## Extrapolation & Stability

It is now possible to create extrapolations of  $u(t)$  using the generative algorithm Algo. 1; the model parameters for FJet are in the center column of Table 4, where  $\epsilon = 0.1$  was used. Using the same  $p(t)$  as was used in the training, Fig. 18 was derived, and

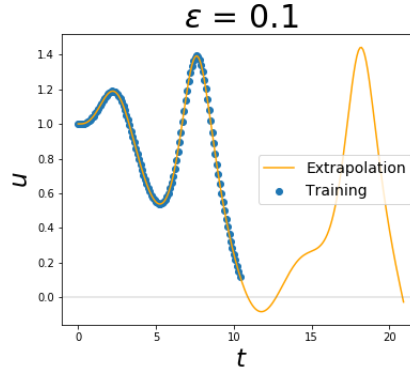


**Figure 18:** A comparison of the extrapolation of FJet to data generated by RK2 over the time range used for the training data  $(0, 2T) \approx (0, 10.5)$ , where  $T = 2\pi/\Omega$  is the period of  $p(t)$ .

illustrates the close match between FJet and the reference solution created with RK2.

The generative algorithm (Algo. 1) in principle does not require the exact same  $p(t)$  as was used in training; recall the training data used only  $p, \dot{p}$ . In principle any smooth function can be used for  $p(t)$ , but for the sake of numerical accuracy, it should be well approximated by its Taylor series expansion for small time steps. To test how well Algo. 1 performed with different parameter values for  $p(t)$ , a comparison was made between RK2 and FJet, where now FJet is trained using  $A = 0.28$ , but is modeled with Algo. 1 using  $A \in (0.10, 0.60)$ . The difference between the two results is computed in

<sup>15</sup>Of course, this is a slight abuse of notation, since derivatives are defined in a limiting procedure.

the function

$$E_n = \max_{t \in (0, nT)} |u_{RK2}(t) - u_{FJet}(t)| \quad (42)$$

which measures the maximum absolute value of the difference, over the time range 0 to  $nT$ , where  $T$  is the period of  $p(t)$ . Plots of  $\log_{10} E_n$  are provided in Fig. 19 for  $n = 10, 20, 30$ , revealing that for times up through about  $30T$ , Algo. 1 provides an

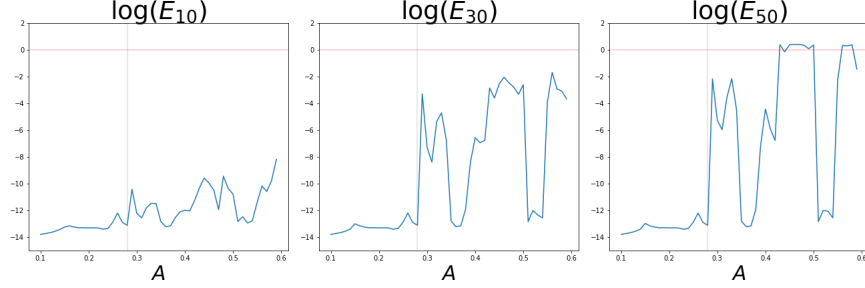


**Figure 19:** Three plots indicating a measure of the error between the extrapolation from FJet compared to the solution from RK2. The left, center and right plots correspond to  $\log_{10} E_n$  (cf. Eq. 42) for  $n = 10, 30$ , and  $50$ , where  $n$  is the number of periods of the driving force.

accurate approximation to RK2, even for values of  $A$  that differ significantly from the value used for training (which is shown as a vertical gray line in the plots. Finally, comparisons were made to RK2, rather than RK4, since the complexity of the model (cf. Eq. 40) was at the level of RK2, as can be better understood after reviewing Appendix A.

### Constants of Motion

Again interpreting  $h_1/\epsilon$  as  $\eta$ , and  $h_2/\epsilon$  as  $\eta^{(1)}$  in the  $\epsilon \rightarrow 0$  limit of the feature regression model, it follows

$$\begin{bmatrix} \eta \\ \eta^{(1)} \end{bmatrix} = \begin{bmatrix} 0 & 1 & 0 & 0 \\ -\alpha & -2\gamma & -\beta & 1 \end{bmatrix} \begin{bmatrix} u \\ \dot{u} \\ u^3 \\ p \end{bmatrix} \quad (43)$$

Following Sec. 2.6, the constant of motion from integration results in

$$\delta r(t) = - \int_{\Gamma} du \eta^{(1)} + \int_{\Gamma} d\dot{u} \eta \quad (44)$$

$$= \delta E - w_p + w_{diss} \quad (45)$$

where

$$\delta E = \int_{\Gamma} du (\alpha u + \beta u^3) + \int_{\Gamma} d\dot{u} \dot{u} \quad (46)$$

$$w_p = \int_{\Gamma} du p \quad (47)$$

$$w_{diss} = 2\gamma \int_{\Gamma} du \dot{u} \quad (48)$$

are computed along the trajectory  $\Gamma(t)$  from  $(u(0), \dot{u}(0))$  to  $(u(t), \dot{u}(t))$ . Here,  $\delta E$  is the change in energy,  $w_p$  is the work done by the external force, and  $w_{diss}$  is the energy lost through dissipation (i.e., because of the damping force). Integrating these quantities along a path in phase space (with initial condition  $((u, \dot{u}) = (0, 0))$ ) yields Fig. 20. Once

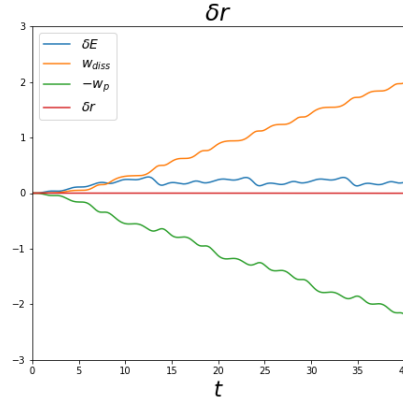


**Figure 20:** Using the initial conditions  $(u, \dot{u}) = (0, 0)$ , and computing the energy, dissipation, and power input along a trajectory as a function of time. Note that the sum of these contributions ( $\delta r$ ) is constant.

again, it is shown that  $\delta r$  is a constant. Also,  $\delta r$  may again be interpreted as the change of the energy of the system and environment, which is zero; it is expressed here, since  $\delta r = 0$ , as  $\delta E = w_p - w_{diss}$ . However, the reader is cautioned that this is not a general feature of this Lie symmetry technique, which doesn't require a physical context.

## 6 Final Remarks

The FJet method has been introduced as an alternative means to model dynamical data, and so derive a model, and in some cases the underlying DE and conserved quantities. It does so by performing ML modeling on updates in the phase space of the system, rather than what competing methods use, a modeling over the time domain. In the FJet approach, the update data is formed by storing differences in the phase space variables over a small time step.

The FJet approach can be understood from the vantage point of a numerical integration scheme Runge-Kutta. By expanding an RK scheme wrt the time step ( $\epsilon$ ), the features appear which are contribute predominantly in modeling. In the examples chosen, expansions of the RK2 scheme were done, and it was possible to know exactly what features should be used in order to identify an equivalence to an RK scheme (RK2 or RK4, e.g.). In the case where an external, time-dependent force was present, it was possible to understand what terms should be additionally included. The result was analogous to a Green's function approach (cf. Eq. 40 for Duffing oscillator). Finally, these considerations led to a general recommendation (Eq. 5) for what features to include, in the normal experimental scenario where the equation of motion isn't known beforehand.

While the modeling in this paper was done exclusively using the feature regression, one should not make the mistake of thinking that it is a requirement. As pointed out in several points in the paper, any ML technique may be used. The reason for using feature regression is that it facilitates determining the underlying DE. If that is not a goal of the researcher, then other ML methods (such as NNs, XG-Boost, Random Forests) become a competitive option.

In the three examples considered, it was demonstrated how the FJet model could lead to extrapolations beyond the range of the original training data. The accuracy of this extrapolation depends upon the number of variables, as well as the quality of the initial data for the updates (i.e.,  $\Delta u$ ,  $\Delta \dot{u}$ ). (Recall that in the examples, this data was created using RK2.)

The initial features that are considered herein are relatively complex (eg,  $v \sin u$  in the Pendulum example) compared to other models, which commonly use a simple polynomial in  $u$ , e.g. It is here asserted by the author that there is an interplay between the complexity of the initial features, and the complexity of the remaining ML model. In particular, it is asserted that for models of comparable (predictive) quality, the sum of these two complexities is constant. The author advocates for models with relatively complex initial features, as they make it easier to train and easier to understand the model (whether the remaining model be relatively simple (regression) or complex (NNs)). Also, the initial features are a good place for the researcher to incorporate any subject matter expertise (e.g., with respect to heuristics, constraints, symmetries, or physical laws).

Other researchers have similarly determined the underlying DE for a dynamical model. However, to the best of the author's understanding, they proceeded by performing a fitting for small time step, while including a regularization term. In contrast, the approach taken here was not to use a regularization, and instead perform several fits at different time steps, and then extrapolate the various coefficients to their value at vanishing time step (i.e.,  $\epsilon \rightarrow 0$ ). In doing this, excellent agreement was seen.

## Acknowledgement

The author kindly acknowledges the insightful instruction on differential equations and dynamical systems from Prof. Julian I. Palmore and Prof. E. Atlee Jackson (d.) at U. Illinois at U.-C. during the author's undergraduate and graduate work there.

## Appendix A: Runge-Kutta

The Runge-Kutta scheme [Press et al., 2007] is a standard technique for the numerical integration of a solution given its ODE. An  $n$ th order ODE which is in Cauchy form (cf. Eq. 1), can be rewritten as a series of first order DEs, and thus the general form for the ODE can be expressed as

$$\frac{dy}{dt} = f(t, y) \quad (49)$$

where  $t(y)$  represents the independent (dependent) variables. The RK scheme involves an update from  $y_n$  to  $y_{n+1}$ , where the difference is

$$\Delta y_n \equiv y_{n+1} - y_n \quad (50)$$

After defining these quantities

$$k_1 = \epsilon f(t_n, y_n) \quad (51)$$

$$k_2 = \epsilon f\left(t_n + \frac{1}{2}\epsilon, y_n + \frac{1}{2}k_1\right) \quad (52)$$

$$k_3 = \epsilon f\left(t_n + \frac{1}{2}\epsilon, y_n + \frac{1}{2}k_2\right) \quad (53)$$

$$k_4 = \epsilon f(t_n + \epsilon, y_n + k_3) \quad (54)$$

the schemes for Euler, RK2 and RK4 can be summarized in Table 5 Note how complexity

Scheme	$\Delta y_n$	Accuracy
Euler	$k_1$	$O(\epsilon^2)$
RK2	$k_2$	$O(\epsilon^3)$
RK4	$\frac{1}{6}(k_1 + 2k_2 + 2k_3 + k_4)$	$O(\epsilon^5)$

**Table 5:** Comment...

is built up in this scheme. For nonlinear ODEs this can lead to many terms involving powers and derivatives of the original variables, as discussed in Sec. 2.4.

In the subsections to follow,  $\Delta y$  will be computed in the RK2 scheme and then expanded with respect to  $\epsilon$ . Since the FJet maps are models of  $\Delta y$ , then this expansion essentially becomes a derivation of the models  $h = (h_1, h_2, \dots)$  in the feature regression technique. In the examples to follow,  $y = (u, \dot{u})$ , and so

$$\Delta y = \begin{bmatrix} \Delta u \\ \Delta \dot{u} \end{bmatrix} = \begin{bmatrix} h_1 \\ h_2 \end{bmatrix}$$

where  $h_1$  and  $h_2$  are functions of  $(u, \dot{u})$ .

## Harmonic Oscillator (damped)

The equation of motion for a damped harmonic oscillator with natural frequency  $\omega_0$  and damping coefficient  $\gamma$  is

$$\ddot{u} = -\omega_0^2 u - 2\gamma \dot{u} \quad (55)$$

Writing  $v = \dot{u}$ , it is equivalent to

$$\begin{bmatrix} \dot{u} \\ \dot{v} \end{bmatrix} = \begin{bmatrix} v \\ -\omega_0^2 u - 2\gamma v \end{bmatrix} = f \left( \begin{bmatrix} u \\ v \end{bmatrix} \right)$$

Note that there is no explicit time dependence in  $f$ . Then the RK2 scheme produces

$$\begin{aligned} \begin{bmatrix} h_1 \\ h_2 \end{bmatrix} &= \epsilon \begin{bmatrix} v - \frac{\epsilon}{2}\omega_0^2 u - \epsilon\gamma v \\ -\omega_0^2(u + \frac{\epsilon}{2}v) - 2\gamma(v - \frac{\epsilon}{2}\omega_0^2 u - \epsilon\gamma v) \end{bmatrix} \\ &= \epsilon \begin{bmatrix} -\frac{\epsilon}{2}\omega_0^2 & 1 - \epsilon\gamma \\ -\omega_0^2(1 - \epsilon\gamma) & -\frac{\epsilon}{2}\omega_0^2 - 2\gamma(1 - \epsilon\gamma) \end{bmatrix} \begin{bmatrix} u \\ v \end{bmatrix} \end{aligned}$$

This shows how the vector  $(u, v)^T$  naturally appears as the features. If RK4 were instead used, terms higher order in  $\epsilon$  would appear in the matrix, but the set of features (i.e.,  $\{u, v\}$ ) would remain the same.

## Pendulum

The equation of motion for the pendulum with natural frequency  $\omega_0$  is

$$\ddot{u} = -\omega_0^2 \sin u \quad (56)$$

After setting  $v = \dot{u}$ , it is equivalent to

$$\begin{bmatrix} \dot{u} \\ \dot{v} \end{bmatrix} = \begin{bmatrix} v \\ -\omega_0^2 \sin u \end{bmatrix} = f \left( \begin{bmatrix} u \\ v \end{bmatrix} \right)$$

Note that there is no explicit time dependence in  $f$ . Then the RK2 scheme produces

$$\begin{bmatrix} h_1 \\ h_2 \end{bmatrix} = \epsilon \begin{bmatrix} v - \frac{\epsilon}{2}\omega_0^2 \sin u \\ -\omega_0^2 \sin(u + \frac{\epsilon}{2}v) \end{bmatrix} \quad (57)$$

$$= \epsilon \begin{bmatrix} 1 & -\frac{1}{2}\epsilon\omega_0^2 & 0 \\ 0 & -\omega_0^2 & -\frac{1}{2}\epsilon\omega_0^2 \end{bmatrix} \begin{bmatrix} v \\ \sin u \\ v \cos u \end{bmatrix} + \mathcal{O}(\epsilon^3) \quad (58)$$

Thus, this expansion in epsilon produces a model akin to the feature regression technique, with the set of predictor variables:  $\{v, \sin u, v \cos u\}$ . If the RK4 were instead used, the reader would find this set to be

$$\{v, \sin u, v \cos u, v^2 \sin u, \sin u \cos u, v^3 \cos u, v \sin^2 u, v \cos^2 u\}$$

Note how the extra terms could arise from the "generating function" given in Eqn. 5.

## Duffing Oscillator

The equation of motion for the Duffing oscillator is

$$\ddot{u} + 2\gamma\dot{u} + \alpha u + \beta u^3 = p(t) \quad (59)$$

where  $p(t) = A \cos \Omega t$  and  $\beta, \gamma > 0$ . Writing  $v = \dot{u}$ , it is equivalent to

$$\begin{bmatrix} \dot{u} \\ \dot{v} \end{bmatrix} = f \left( t, \begin{bmatrix} u \\ v \end{bmatrix} \right) = \begin{bmatrix} v \\ -2\gamma v - \alpha u - \beta u^3 + p(t) \end{bmatrix}$$

Note that in this case there is explicit time dependence in  $f$  due to  $p(t)$ . The RK2 scheme produces

$$\begin{aligned} \begin{bmatrix} h_1 \\ h_2 \end{bmatrix} &= \epsilon \begin{bmatrix} (1 - \epsilon\gamma)v - \frac{\epsilon}{2}\alpha u - \frac{\epsilon}{2}\beta u^3 + \frac{\epsilon}{2}p(t) \\ -2\gamma(1 - \epsilon\gamma)v - \frac{\epsilon}{2}\alpha v - \alpha(1 - \epsilon\gamma)u + \epsilon\beta\gamma u^3 - \beta(u + \frac{\epsilon}{2}v)^3 - \epsilon\gamma p(t) + p(t + \frac{\epsilon}{2}) \end{bmatrix} \\ &= \epsilon \begin{bmatrix} (1 - \epsilon\gamma) & -\frac{\epsilon}{2}\alpha & -\frac{\epsilon}{2}\beta & 0 & \frac{\epsilon}{2} & 0 \\ -2\gamma(1 - \epsilon\gamma) - \frac{\epsilon}{2}\alpha & -\alpha(1 - \epsilon\gamma) & -\beta(1 - \epsilon\gamma) & -\frac{3\epsilon}{2}\beta & (1 - \epsilon\gamma) & \frac{\epsilon}{2} \end{bmatrix} \begin{bmatrix} v \\ u \\ u^3 \\ u^2v \\ p \\ \dot{p} \end{bmatrix} + O(\epsilon^3) \end{aligned}$$

where  $\dot{p}$  denotes the time derivative of  $p$ . Thus, this numerical integration scheme implies the vector of predictor variables  $X = (v, u, u^3, u^2v, p, \dot{p})^T$  if feature regression modeling is used.

## General Expansion

Consider the above cases, where there is no explicit time dependence. In that case, the  $k_i$  can be written

$$k_{i+1} = \epsilon f \left( \begin{bmatrix} u + \delta u_i \\ v + \delta v_i \end{bmatrix} \right)$$

where  $i = 1, 2, 3$  and  $k_1$  is just  $\epsilon f$ . Now use subscripts  $a, b$  to identify the top ( $a$ ) and bottom ( $b$ ) components of the 2-by-1 vector:

$$\begin{aligned} \delta u_1 &= (1, 0) \begin{bmatrix} \frac{1}{2}k_1 \\ \frac{1}{2}k_1 \end{bmatrix} \equiv \left(\frac{1}{2}k_1\right)_a = \frac{\epsilon}{2}f_a = \frac{\epsilon}{2}v \\ \delta v_1 &= (0, 1) \begin{bmatrix} \frac{1}{2}k_1 \\ \frac{1}{2}k_1 \end{bmatrix} \equiv \left(\frac{1}{2}k_1\right)_b = \frac{\epsilon}{2}f_b = -\frac{\epsilon}{2}\sin u \end{aligned}$$

Likewise,

$$\begin{aligned} \delta u_2 &= \left(\frac{1}{2}k_2\right)_a \\ \delta v_2 &= \left(\frac{1}{2}k_2\right)_b \\ \delta u_3 &= (k_3)_a \\ \delta v_3 &= (k_3)_b \end{aligned}$$

Using the expression for  $k_{i+1}$  and expanding it with respect to  $\delta u_i$  and  $\delta v_i$ , and taking advantage of the fact that in this example many of the partial derivatives of  $f$  with respect to  $u, v$  are zero, one obtains

$$k_{i+1} = \epsilon \left\{ f + \delta u_i \partial_u f + \delta v_i \partial_v f + \frac{1}{2!} (\delta u_i)^2 \partial_u^2 f + \frac{1}{3!} (\delta u_i)^3 \partial_u^3 f + \dots \right\}$$

where  $\partial_u f = \partial f / \partial u$ , etc. This expansion is stopped at third order, because higher orders will lead to contributions beginning at  $\mathcal{O}(\epsilon^5)$ . These are ignored since RK4 is an  $\mathcal{O}(\epsilon^5)$  algorithm.

The point of doing this expansion is to demonstrate how low complexity models might be motivated, from the standpoint of a numerical integration scheme. The above equation shows that all manner of monomials result, involving the original feature set and various derivatives of them. Also, keep in mind that the complexity builds on this, since  $k_1$  gets substituted into  $k_2$ , and then  $k_3$  and  $k_4$ . It is this expansion which is the motivation for the guidance given in Eq. 5.

## Appendix B: Stability – Harmonic Oscillator

The stability is now analyzed by focusing on a conserved quantity, the energy  $E = \frac{1}{2}(u^2 + \dot{u}^2)$ , where now  $\omega_0 = 1$  and  $\gamma = 0$ . Following Young [2020], the energy at the  $n$ th step ( $E_n$ ) may be expressed as <sup>16</sup>

$$2E_n = r^{2n} = e^{(\log r^2)n} = e^{\lambda n} \quad (60a)$$

$$r^2 = (1 + a_1)^2 + a_2^2 \quad (60b)$$

where the initial condition of  $(u, \dot{u}) = (1, 0)$  is used. Thus, the key quantity is  $\lambda = \log r^2$ ; it measures the exponential growth/decay of  $E$ . Of course, the best choices for  $a_1, a_2$  would lead to  $r = 1$ , so that  $\lambda = 0$ . Formulae for  $a_1, a_2$  from Appendix A due to Euler/RK2/RK4 are given in Table 6. The values they lead to, along with the values for

	<b>Euler</b>	<b>RK2</b>	<b>RK4</b>
$a_1$	0	$-\epsilon^2/2$	$-\epsilon^2/2 + \epsilon^4/24$
$a_2$	$\epsilon$	$\epsilon$	$\epsilon - \epsilon^3/6$

**Table 6:** Values for  $a_1, a_2$  for the Euler/RK2/RK4 integration schemes.

them due to the FJet method, are given in Table 7. Upon substituting these values into Eq.60b and computing  $\lambda = \log(r^2)$ , the values for Table 2 are produced.

<sup>16</sup>The correspondence between  $(a, b)$  as defined here corresponds to  $(c, d)$  in Young [2020] via  $(a, b) = (c - 1, d)$ . Also note that his matrix is for an update on a variable  $(u, v)$ , whereas here it is for *differences* in those variables.

	<b>Euler</b>	<b>RK2</b>	<b>RK4</b>	<b>FJet</b>
$a_1$	0	-0.005	-0.004995833	-0.004995834721974124
$a_2$	0.1	0.1	0.099833	0.09983341664682731

**Table 7:** Values for  $a_1, a_2$  using  $\epsilon = 0.1$  for the Euler/RK2/RK4 schemes, based on expressions from Table 6. Also included are the values for the FJet method.

## Appendix C: Derivation of $r$ for Damped Oscillator

Rather than working directly on

$$\begin{bmatrix} du \\ dv \end{bmatrix} = A \begin{bmatrix} u \\ v \end{bmatrix} \epsilon \quad (61)$$

where

$$A = \begin{bmatrix} 0 & 1 \\ -\omega_0^2 & -2\gamma \end{bmatrix}$$

the approach will be to first transform  $A$ . It is diagonalized as  $A = S\Lambda S^{-1}$ , where

$$S = \begin{bmatrix} 1 & 1 \\ \lambda_+ & \lambda_- \end{bmatrix}$$

$$\Lambda = \begin{bmatrix} \lambda_+ & 0 \\ 0 & \lambda_- \end{bmatrix}$$

$$S^{-1} = \frac{1}{2} \begin{bmatrix} 1 - i\gamma/\omega & -i/\omega \\ 1 + i\gamma/\omega & i/\omega \end{bmatrix}$$

Upon defining

$$\begin{bmatrix} \bar{u} \\ \bar{v} \end{bmatrix} = S^{-1} \begin{bmatrix} u \\ v \end{bmatrix}$$

and similarly for  $du, dv$ , Eq. 61 becomes transformed to

$$\begin{bmatrix} d\bar{u} \\ d\bar{v} \end{bmatrix} = \Lambda \begin{bmatrix} \bar{u} \\ \bar{v} \end{bmatrix} \epsilon$$

Following the approach of Sec. 2.6, the constant of motion is found through integration to be

$$r = \gamma \ln \left( \frac{\bar{u}}{\bar{v}} \right) + i\omega \ln (\bar{u}\bar{v})$$

where

$$\bar{u} = a - ib$$

$$\bar{v} = a + ib$$

$$a = u/2$$

$$b = (\gamma u + v)/(2\omega)$$

$$r' = \ln \left[ \frac{1}{2} \omega^2 u^2 + \frac{1}{2} (\gamma u + v)^2 \right] + \frac{2\gamma}{\omega} \phi_n - \ln(2\omega^2)$$

with  $\tan \phi_n = -b/a$ .

## References

- H. Poincaré. Sur les courbes définies par une équation différentielle. *Journal de Mathématiques Pures et Appliquées*, 4(1):167–244, 1885.
- P. Holmes. Poincaré, celestial mechanics, dynamical-systems theory and “chaos”. *Physics Reports*, 193(3):137–163, 1990.
- H. Poincaré. *New Methods of Celestial Mechanics, 1: Periodic and Asymptotic Solutions* (Ed. D.L. Goff). American Institute of Physics, 1993.
- N.H. Packard, J.P. Crutchfield, J.D. Farmer, and R.S. Shaw. Geometry from a time series. *Physical Review Letters*, 45, 1980.
- F. Takens. Detecting strange attractors in turbulence. In *Lecture Notes in Mathematics: Dynamical Systems and Turbulence, Warwick 1980 (Coventry, 1979/1980)*, volume 898, pages 366–381. Springer, 1981.
- J.P. Crutchfield and B.S. McNamara. Equations of motion from a data series. *Complex Systems*, 1:417–452, 1987.
- D.S. Broomhead and D. Lowe. Multivariable functional interpolation and adaptive networks. *Complex Systems*, 2(3):321–355, 1988.
- M. Casdagli. Nonlinear prediction of chaotic time series. *Physica D*, 35(3):335–356, 1989.
- J. Cremers and A. Hübler. Construction of differential equations from experimental data. *Zeitschrift für Naturforschung A*, 42(8):797–802, 1987.
- J.L. Breeden and A. Hübler. Reconstructing equations of motion from experimental data with unobserved variables. *Physical Review A*, 42, 1990.
- G. Gouesbet. Reconstruction of vector fields: the case of the lorenz system. *Physical Review A*, 46(4):1784–1796, 1992.
- L.A. Aguirre and C. Letellier. Modeling nonlinear dynamics and chaos: A review. *Mathematical Problems in Engineering*, 2009, 2009.
- M. Lutter, C. Ritter, and J. Peters. Deep Lagrangian Networks: Using physics as model prior for deep learning. In *International Conference on Learning Representations (ICLR)*, 2019.
- M. Cranmer, S. Greydanus, S. Hoyer, P. Battaglia, D. Spergel, and S. Ho. Lagrangian neural networks. *arXiv preprint*, arXiv:2003.04630, 2020.

- S. Greydanus, M. Dzamba, and J. Yosinski. Hamiltonian neural networks. In *Neural Information Processing Systems (NeurIPS)*, pages 15353–15363, 2019.
- P. Toth, D.J. Rezende, A. Jaegle, S. Racanière, A. Botev, and I. Higgins. Hamiltonian generative networks. volume arXiv:1909.13789, 2019.
- S.H. Rudy, S.L. Brunton, J.L. Proctor, and J.N. Kutz. Data driven discovery of partial differential equations. *Science Advances*, 3(4), 2017.
- Z. Liu, B. Wang, Q. Meng, W. Chen, M. Tegmark, and T.-Y. Liu. Machine-learning non-conservative dynamics for new-physics detection. *arXiv preprint*, arXiv:2106.00026, 2021.
- F. John. *Partial Differential Equations*. Springer-Verlag, 4th edition, 1982.
- E. DiBenedetto. *Partial Differential Equations*. Birkhauser, 2 edition, 2009.
- P.J. Olver. *Applications of Lie Groups to Differential Equations*. Springer-Verlag, 2nd edition, 1993.
- P.E. Hydon. *Symmetry Methods for Differential Equations: A Beginner's Guide*. Cambridge, 2000.
- G.W. Bluman and S. Kumei. *Symmetries and Differential Equations*. Springer-Verlag, 1989.
- A.P. Young. Physics 115/242, Comparison of methods for integrating the simple harmonic oscillator, 2020. URL [https://young.physics.ucsc.edu/115/ode\\_solve.pdf](https://young.physics.ucsc.edu/115/ode_solve.pdf).
- T. Hastie, R. Tibshirani, and J. Friedman. *The Elements of Statistical Learning: Data Mining, Inference, and Prediction*. Springer-Verlag, 2nd edition, 2009.
- G. Duffing. Erzwungene schwingungen bei veränderlicher eigenfrequenz und ihre technische bedeutung" [forced oscillations with variable natural frequency and their technical relevance]. *Vieweg, Braunschweig*, 41/42, 1918.
- F.C. Moon and P.J. Holmes. A magnetoelastic strange attractor. *Journal of Sound and Vibration*, 65:275–296, 1979.
- E. Atlee Jackson. *Perspectives of nonlinear dynamics*, volume 1. Cambridge University Press, 1991.
- W.H. Press, S.A. Teukolsky, W.T. Vetterling, and B.P. Flannery. *Numerical Recipes, The Art of Scientific Computing*. Cambridge University Press, 3rd edition, 2007.